Femtosecond Heterodyne-Detected Four-Wave-Mixing Studies of Deterministic Protein Motions. 1. Theory and Experimental Technique of Diffractive Optics-Based Spectroscopy

Gregory D. Goodno[†]

Department of Physics and Astronomy, University of Rochester, Rochester, New York 14627

R. J. Dwayne Miller*

Departments of Chemistry and Physics, 80 St. George Street, University of Toronto, Toronto, Ontario M5S 3H6, Canada

Received: July 27, 1999; In Final Form: October 5, 1999

Analytic relations are developed to describe the coupling between experimentally observed optically heterodyne-detected (OHD) transient grating (TG) signals and the underlying molecular dynamics of heme proteins. The heterodyne detection was implemented using a diffractive optical element to generate the phase-matched beam pattern along with a reference beam for OHD. The phase stability between the reference and signal fields using this approach is shown to be excellent over several hours of signal collection. Under small signal conditions this leads to an enhancement in signal-to-noise of several orders of magnitude. The grating excitation provides an inherent acoustic reference that can be used to determine the absolute signal phase. This enables separation of the real and imaginary components to the nonlinear susceptibility as well as determination of both the absorption anisotropy and its real counterpart, the phase anisotropy. The relationship between the phase anisotropy and the observed OHD TG signals is expressed in terms of the complex molecular polarizability specific to heme proteins but can be readily extended to all other systems. Access to the material anisotropy provides a direct probe of mode selective coupling in proteins, i.e., the nonuniform displacements determined by the underlying asymmetric protein structure.

I. Introduction

Protein dynamics are intimately connected to the structure/function relationship of biological systems. The causal connection between dynamics and function highlight interesting problems in scaling. For example, the breaking or making of a chemical bond at an active site is most strongly influenced by force fields very local to the reaction center. However, for numerous biological processes, the ensuing protein structural changes accompanying the reaction must spatially extend out to the mesoscopic dimensions of the protein to execute a biological function. The quandary is that proteins are highly associated systems and have innumerable minima nested within an extremely complex potential energy landscape.[1] A statistical sampling of all degrees of freedom available to such large molecules would lead to time scales for reactive crossings many orders of magnitude slower than observed.[2,3] Somehow biological systems have found a way to transduce forces that develop on an atomic length scale to length scales an order of magnitude larger or more. The reaction and overall sequence of events are obviously highly directed. The question is what is the "director" in this sampling process.[3] The specific asymmetric structure of the protein is expected to be the primary agent, but the mechanics of the coupling of the reaction forces to the different length scales of motions is not well understood.

One of the classic problems in this regard is the mechanism of molecular cooperativity exhibited by hemoglobin.[4] Hemoglobin is composed of four nearly identical heme protein subunits with approximately 1200 atoms each and diameters of ∼30 Å. Each subunit is capable of binding one oxygen molecule per heme Fe. This protein complex undergoes a factor of 300 change in oxygen binding affinity that depends on the number of oxygen molecules bound at the Fe sites. The Hill coefficient of cooperativity is approximately 3.[4] This value indicates phenomenologically that the binding of oxygen at all four sites affects the oxygen binding at neighboring sites. The interaction between protein subunits produces more than a 20 dB gain in response to changes in the partial pressure of oxygen about a critical value. This synergistic coupling of reaction coordinates and effect on the rate of oxygen binding is essential to transporting oxygen from the lungs to extremities in the body. The simplest model to explain the interaction between the heme protein subunits is the use of a two-state model, as first proposed by Monod et al.[5] In this model, it was proposed that there was a transition from a low-efficiency to high-efficiency binding state. From the pioneering work of Perutz,[6] it was later determined that the structure of fully oxygenated hemoglobin and fully deoxyhemoglobin are different.[4] The remarkable finding from these crystallographic studies was that the two structures varied in their quaternary structure by as much as 15° ball-in-socket type rotation and 6 Å translation about the interfacial contact region. There was the apparent explanation for the Monod Two-State Model. The switch between the high-affinity (R) and low-affinity (T) forms was correlated to the changes in quaternary structure. There are also distinctive changes in structure at the tertiary level, but the quaternary changes are the most significant and are thought to dominate the modulation of the activation barrier to binding of oxygen.

[†]Current address: TRW Space and Electronics Group, Redondo Beach, CA 90278.

10.1021/jp992597e CCC: $18.00
Published on Web 11/12/1999

The phenomena of molecular cooperativity is derived from structural changes that literally involve 10^4 degrees of freedom or more and is powered by one or a few chemical bonds. The hemoglobin example is representative of a large class of allosteric enzymes that exhibit changes in activity with changes in configuration.[6] Similar long-range correlations with small input energies exist for all protein systems that rely on some level of locomotion to perform their function. These protein systems must be poised to highly direct the reaction forces to their respective functionally relevant motions. Again, using hemoglobin as the model system, an "allosteric core" has been identified within the asymmetric structure of the heme protein subunits.[7] The steepest potential energy gradient is found to be along the EF helical section in intimate contact with the protein−protein interface and the ligand binding site at the iron. Thus, the reaction force is highly anisotropic and should lead to larger displacements along the direction required for intersubunit communication. Displacements along this tertiary coordinate effectively transfer forces from the binding site to the protein contact region and ultimately couples the reaction sites through fluctuations along the quaternary coordinate. In other words, there is a built-in gradient in the asymmetric protein structure that directs the process. With respect to the length scale vs time scale debate, the mechanism by which such highly associated systems, with so many degrees of freedom, samples this coordinate is the fundamental issue.[3]

To fully understand this problem, information on both the structural changes and the degree of coupling of the reaction coordinate to different modes/relaxation processes of the protein system is needed. The ultimate experiment would be to perform time-resolved diffraction experiments. Recently, there has been remarkable progress toward this goal.[8] Even in this event, it is difficult to connect the structural changes to the energetics of the relaxation process. The energetics are essential to distinguishing a dominant relaxation phase in connection with the mode selective coupling inherent to a highly directed process. Moreover, the structural relaxations thought to be most important to function often involve highly correlated motions with very small displacements (e.g., <0.1 Å for the motions of the EF helical sections of myoglobin).[4,6,8] It is desirable to have an experimental method that is sensitive enough to detect the smallest motions, ultimately down to the level of the background thermal fluctuations, and one that can be connected to the energetics of the relaxation process.

In this paper, we expand on an earlier report on the use of heterodyne-detected transient grating spectroscopy to follow these motions with the prerequisite sensitivity.[9] The observable is the density change or protein strain (ΔS) that accompanies protein relaxation. This aspect to the observable is contained within the real part of the nonlinear susceptibility. Assuming linear response, the strain variable can be connected to the change in the potential energy of the protein as it relaxes (i.e., the observable is the protein strain energy). The sensitivity of this approach is now well within the range to follow the most minute motions. Changes in effective volume of less than 0.01 Å in effective radius can now be detected ($\Delta S \leq 10^{-6}$) with heterodyne amplification of the signal. For comparison the smallest root mean square (rms) thermal fluctuations of the helical regions, as determined from Debye−Waller factors, are on the order of 0.03 Å.[10] The current sensitivity is well within the thermal limit such that the even the smallest motions leading to protein strain are detectable.

The new feature of this spectroscopy is the use of diffractive optics to provide a phase-locked reference field for mixing with the signal field.[9,11,12] This possibility was first suggested by the work of Rogers and Nelson that employed transmission gratings to provide the correct beam pattern.[13] This seminal work focused on the ease of alignment and direct detection of the signal. We expanded on this concept and explored the use of surface relief diffractive optics to obtain high transfer efficiency of the incoming light to the desired beam pattern ($\geq 75\%$ at the design wavelength) and provide the most stable reference possible for mixing with the signal field using a diffractive optic.[11] The diffraction process off the surface profile defines the phases of the excitation, probe, and reference fields and is precisely defined at the surface. As long as the extracted beams all pass through the same optics, this single optic provides passive phase locking of these different optical fields on par or superior to active feedback methods. As will be shown below, this approach can achieve signal enhancements of several orders of magnitude in the small signal limit, as expected for true phase-locked mixing of the reference and signal fields.

The advantages of heterodyne detection are linearization of the signal, enhancement of the small signal detection limit by orders of magnitude, and separation of the real and imaginary contributions to the complex nonlinear susceptibility. The latter attribute is the most important to the present study. The conventional method of measuring the diffracted probe intensity alone (direct detection) gives a signal proportional to the modulus squared of the complex nonlinear susceptibility. The signal scales quadratically and contains contributions from both amplitude and phase grating contributions, i.e., excitation-induced variations in absorption (imaginary) and the index of refraction (real) at the grating wave vector, respectively. As discussed, the mass displacements associated with protein motions contribute to changes in the index of refraction or the real part of the nonlinear susceptibility. For probe wavelengths well off resonance, the protein contribution to the grating signal can be significant or even dominate the signal. However, it is desirable to cleanly separate the two contributions to avoid complications from different sources for the diffracted signal. Separation of the amplitude and phase grating contributions is achieved by using an internal acoustic reference to set the relative phase differences between the reference and signal fields.[9,12] The high phase stability of this approach greatly facilitates this operation. This new ability makes it possible to directly observe protein motion coupled to the reaction coordinate with even higher sensitivity than previous studies. The clean separation of the real and imaginary components also makes it possible to define a phase anisotropy in analogy to absorption anisotropy.[9] The above issue of directionality in biological molecules requires that the mass displacement in response to reaction forces be anisotropic. The prospect of determining the phase anisotropy provides a direct observation of this mode selective coupling. Thus, it not only provides the opportunity to directly observe the modes/relaxation processes coupled to the reaction coordinate but also casts out those motions that can be assigned as the functionally most important motions.

In this first paper of a two-part series, we analyze the relationship between the experimental OHD TG signals and the underlying molecular geometry and dynamics, and we show how polarization resolution of the TG signals enables measurement of anisotropic strain in the protein. A description of previously unreported aspects of the experimental heterodyne setup using a diffractive optical element for passive phase stabilization is also provided here, along with a comparison to previous work using active stabilization. The experimental

results obtained by applying these methods to heme proteins will be discussed in detail in the second paper.[14]

II. Theory

A. Relation between the Molecular Index Ellipsoid and the Grating Signals. The macroscopic sample is taken to be an ensemble of independent (noninteracting) protein molecules in dilute solution. The grating signals can be expressed as changes in the linear susceptibility, as this formalism allows the complex material response to be written using relatively compact expressions. Since the protein contribution is viewed as a small perturbation to the real, isotropic solvent susceptibility, there is a simple relation to the more commonly used index of refraction and absorption ellipsoids:[15]

$$n_{ij} = \delta_{ij} n_0 + \frac{\mathrm{Re}(\chi_{ij})}{2n_0} \tag{1}$$

$$\alpha_{ij} = -\frac{\omega\ \mathrm{Im}(\chi_{ij})}{cn_0} \tag{2}$$

Here n_0 is the isotropic contribution to the refractive index from the solvent, ω is the optical frequency, c is the speed of light, δ_{ij} is the Kronecker delta function, and χ_{ij} refers to the protein contribution to the susceptibility only. Equations 1 and 2 are written relative to the molecular coordinates of a single molecule, taken to be the eigenbasis of the imaginary (Im) part of the protein susceptibility. It is well-known that in their ground state heme proteins are to a very good approximation "planar absorbers" in the visible part of the spectrum.[16] This means that the molecule has appreciable polarizability only in the plane of the heme ring and can only interact with the component of an applied field that is within the heme plane. Written explicitly in the molecular eigenbasis, the anisotropic susceptibility for a planar absorber in the ground state is

$$\mathrm{Im}[\chi^{g}(\omega)] = \mathrm{Im}[\chi^{g}(\omega)]\begin{pmatrix} 0 & 0 & 0 \\ 0 & 1 & 0 \\ 0 & 0 & 1 \end{pmatrix} \tag{3}$$

where the superscript g refers to the ground state.

The Euler rotation matrix $\mathbf{R}(\Omega)$, with $\Omega \equiv (\varphi,\theta,\psi)$, defines a mapping of the molecular eigenbasis into the laboratory coordinate system as shown in Figure 1a,[17] so that in the lab frame the molecular susceptibility is

$$\chi(\Omega,\omega) = \mathbf{R}^{-1}(\Omega)\cdot\chi(\omega)\cdot\mathbf{R}(\Omega) \tag{4}$$

The laboratory coordinate system used in this analysis is shown in Figure 1b. The $\mathbf{u}_1$ direction is along the grating wavevector formed by the intersection of the two input excitation fields $\mathbf{E}^{ex1}$ and $\mathbf{E}^{ex2}$, with wavevectors $\boldsymbol{k}_1$ and $\boldsymbol{k}_2$:

$$\mathbf{u}_1 = \frac{\mathbf{k}_1 - \mathbf{k}_2}{|\mathbf{k}_1 - \mathbf{k}_2|} \tag{5}$$

The $\mathbf{u}_2$ axis is in the plane of the grating (the sample plane as shown), and the $\mathbf{u}_3$ axis is along the optic axis of the experiment. We define the polarization angles of all four fields involved in the grating experiment with respect to the $\mathbf{u}_1$ axis as shown in Figure 1. The approximation (valid in the limit of small crossing angles between beams) is made that none of the fields have appreciable vector components along the optic axis $\mathbf{u}_3$.

Assuming a two-level system, basic considerations of Maxwell's equations[18] lead to an expression for the probability

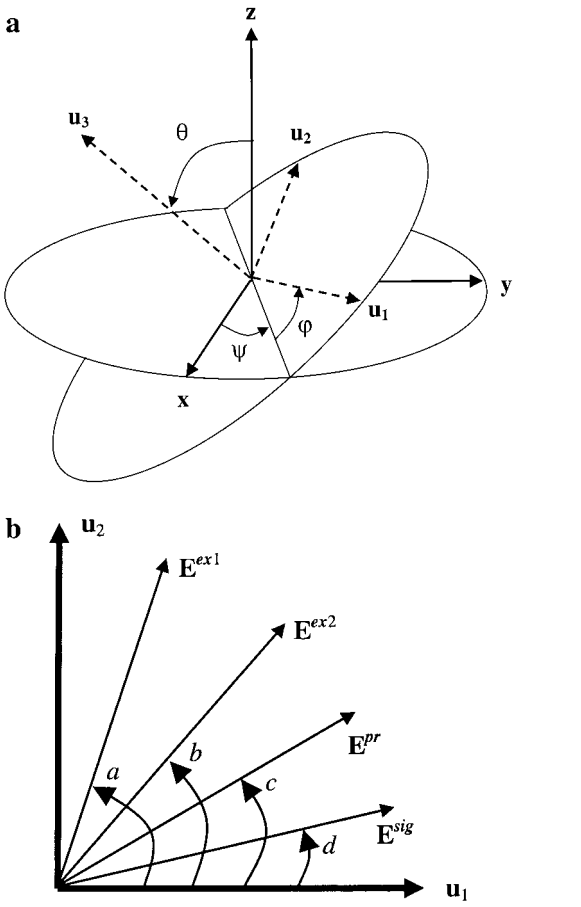

Figure 1. Laboratory coordinate system for analysis of the transient grating experiment. (a) The set of Euler angles $\Omega = (\varphi, \theta, \psi)$ that defines the relationship between the molecular axes (**x**, **y**, **z**) and the laboratory coordinate system ($\mathbf{u}_1$, $\mathbf{u}_2$, $\mathbf{u}_3$). The horizontal oval represents the heme plane, with **x** and **y** within the plane and **z** along the heme normal. The tilted oval represents a plane that is square along the lab coordinates, with $\mathbf{u}_3$ the optic axis along which the laser beams propagate, and $\mathbf{u}_1$ and $\mathbf{u}_2$ the two transverse directions. (b) Polarization angles (a, b, c, d) of the four optical fields ($\mathbf{E}^{ex1}$, $\mathbf{E}^{ex2}$, $\mathbf{E}^{pr}$, $\mathbf{E}^{sig}$). The fields are assumed to have no component along $\mathbf{u}_3$ (small crossing angle limit).

density $p_e(\Omega,\omega)$ for exciting a molecule of orientation Ω from the ground state g to the excited state e through absorption of the total applied excitation field $\mathbf{E}^{ex1} + \mathbf{E}^{ex2}$:

$$p_e(a,b,u_1,\Omega,\omega_{ex}) = C_{ex}\omega_{ex}\mathrm{Im}\{[\mathbf{E}^{ex1}(a,u_1) + \mathbf{E}^{ex2}(b,u_1)]^{*}\cdot\chi^{g}(\Omega,\omega_{ex})\cdot[\mathbf{E}^{ex1}(a,u_1) + \mathbf{E}^{ex2}(b,u_1)]\} \tag{6}$$

Here ω_{ex} is the optical frequency of the excitation pulses, and a and b are defined in Figure 1b. C_{ex} is a normalization constant such that the probability of the molecule remaining in the ground state is $p_g(a,b,u_1,\Omega,\omega_{ex}) = 1 - p_e(a,b,u_1,\Omega,\omega_{ex})$. This expression is only valid in the small-field limit, where there is negligible depletion of the ground state. For simplicity we assume optically thin samples, so that the excitation intensity does not vary as a function of propagation depth within the sample (u_3). The only part of the photoselected distribution that can contribute to a grating signal is the change in the distribution across a half grating fringe $\Lambda/2 = \pi/|\mathbf{k}_1 - \mathbf{k}_2|$, i.e., the difference in the distribution between illuminated and dark fringes:

$$\Delta p_e(a,b,\Omega,\omega_{ex}) = p_e(a,b,0,\Omega,\omega_{ex}) - p_e(a,b,\Lambda/2,\Omega,\omega_{ex}) \tag{7}$$

In the coordinate system of Figure 1, the excitation fields are

$$\mathbf{E}^{\mathrm{ex1}}(a,u_1) = E^{\mathrm{ex1}} \exp(\mathrm{i}\pi u_1/\Lambda)[\cos(a)\mathbf{u_1} + \sin(a)\mathbf{u_2}] \quad (8)$$

$$\mathbf{E}^{\mathrm{ex2}}(b,u_1) = E^{\mathrm{ex2}} \exp(-\mathrm{i}\pi u_1/\Lambda)[\cos(b)\mathbf{u_1} + \sin(b)\mathbf{u_2}] \quad (9)$$

where E^{ex1} and E^{ex2} are constant (or slowly varying) amplitudes. Both fields are assumed to be linearly polarized. The origin of u_1 is defined so that the two input excitation fields are in phase at $u_1 = 0$. Substituting eqs 3, 4, 6, 8, and 9 into eq 7, the photoselected distribution that gives rise to a grating signal is

$$\Delta p_{\mathrm{e}}(a,b,\Omega,\omega_{\mathrm{ex}}) = 4E^{\mathrm{ex1}}E^{\mathrm{ex2}}{}^{*}C_{\mathrm{ex}}\omega_{\mathrm{ex}}\,\mathrm{Im}[\chi^{\mathrm{g}}(\omega_{\mathrm{ex}})]\{[1 - R_{11}{}^{2}(\Omega)]\cos(a)\cos(b) + [1 - R_{12}{}^{2}(\Omega)]\sin(a)\sin(b) - R_{11}(\Omega)\,R_{12}(\Omega)[\cos(a)\sin(b) + \cos(b)\sin(a)]\} \quad (10)$$

where $R_{ij}(\Omega)$ is the ijth element of the Euler rotation matrix $\mathbf{R}(\Omega)$.[17]

Next we need to determine the contribution from a single excited molecule to the change in the linear susceptibility experienced by the probe beam. To determine the explicit form of this tensor, we will consider separately the different physical effects that can couple to the susceptibility. Since we are considering changes in a linear optical property of the medium, we can simply sum the contributions from each effect independently to find the total susceptibility change at the probe wavelength from a single excited molecule:

$$\Delta\chi = \Delta\chi^{\mathrm{elect}} + \Delta\chi^{\mathrm{sol}} + \Delta\chi^{\mathrm{glob}} \quad (11)$$

Here, $\Delta\chi^{\mathrm{elect}}$ is the susceptibility change from electronic dipole interactions at the probe wavelength, i.e., the difference in the polarizabilities of the ground and excited states at the probe wavelength:

$$\Delta\chi^{\mathrm{elect}} = \chi^{\mathrm{e}}(\omega_{\mathrm{pr}}) - \chi^{\mathrm{g}}(\omega_{\mathrm{pr}}) \quad (12)$$

At the 800-nm probe wavelengths used here, the absorption ellipsoid of the heme can have nonzero components along any molecular axis, so the ground- and excited-state susceptibilities must be kept general with six independent elements.

$\Delta\chi^{\mathrm{sol}}$ is the change in the susceptibility due to temperature or density fluctuations in the bulk solvent. These changes are a secondary effect in that we assume the solvent does not couple directly to the excitation field but only indirectly via the protein−field interaction. The bulk solvent properties may change due to thermalization of excess photon energy beyond that required to break the heme−ligand bond, or possibly due to changes in the volume element occupied by the protein molecule. These changes are optically isotropic,[19] so that $\Delta\chi^{\mathrm{sol}}$ is simply proportional to the identity (unit) matrix $\mathbf{I}$:

$$\Delta\chi^{\mathrm{sol}} = \Delta\chi^{\mathrm{sol}}\mathbf{I} \quad (13)$$

Note that eq 13 does not imply that the solvent response is homogeneous. It is indeed true that there will be nonuniform local variations in the solvent density that are driven by the nonuniform local displacement of the protein. However, a variation in local solvent density will still couple isotropically to the macroscopic susceptibility since there is no preferred orientation or packing of the solvent molecules with respect to the protein. A local density change in the solvent means that the average distance between solvent molecules has changed. Unless this average distance between molecules is different along different directions (i.e., solvent molecules are packed tightly along one dimension but spaced far apart from one another along another direction), then the solvent response will be optically isotropic. Experimentally, the optical isotropy of the solvent response is demonstrated by the lack of photoacoustic oscillations in the direct-detected χ_{1212} tensor element (excitation with crossed polarizations).[9]

This should be contrasted with the optical response of the protein $\Delta\chi^{\mathrm{glob}}$. Within the protein molecule, atoms are indeed compressed (or rarefied) more along one direction than along another, resulting in an observable anisotropic response. The two physical changes in the protein upon photodissociation of the heme−ligand bond are conformational relaxation and a shift in temperature. If the change in the protein geometry gives rise to a direct interaction with the probe beam, this interaction may be anisotropic. Since the globin is far off-resonance for optical frequencies in the visible−near-IR range, it is highly unlikely that there will be any noticeable change in absorption in this wavelength regime upon conformational relaxation. Thus, we can safely assume $\mathrm{Im}(\Delta\chi^{\mathrm{glob}}) = 0$; i.e., the contribution of the globin to the grating signals is purely real. The globin evolution may indirectly result in an absorption change by perturbing the electronic structure of the heme.[20,21] However, we shall consider this effect to be included in the electronic contribution of eq 12 instead. Since the susceptibility change for the globin contribution is a priori unknown, it too must be kept general, with six independent elements.

The contribution to the change in the linear bulk susceptibility from a single molecule of orientation Ω can be seen by writing eq 11 in the lab frame as per eq 4:

$$\Delta\chi_{ij}(\Omega) = \Delta\chi^{\mathrm{sol}}\delta_{ij} + \sum_{kl}[\chi^{\mathrm{e}}_{kl}(\omega_{\mathrm{pr}}) - \chi^{\mathrm{g}}_{kl}(\omega_{\mathrm{pr}}) + \chi^{\mathrm{glob}}_{kl}]R_{ki}(\Omega)R_{lj}(\Omega) \quad (14)$$

The macroscopic susceptibility change is the contribution from each molecule $\Delta\chi(\Omega)$ weighted by the photoselection probability $\Delta p_{\mathrm{ex}}(a,b,\Omega)$ and averaged over all possible orientations (assuming an initially isotropic orientational distribution). This is explicitly a function of the excitation field orientations:

$$\Delta\chi^{\mathrm{eff}}(a,b) = \int \mathrm{d}\Omega\; \Delta p_{\mathrm{ex}}(a,b,\Omega)\Delta\chi(\Omega) \quad (15)$$

Inserting eqs 10 and 14 and performing the angular integrals yields expressions for the elements of the linear bulk susceptibility change in terms of distinct physical contributions to the molecular polarizability. To within a global multiplicative constant, the on-diagonal elements are

$$\Delta\chi^{\mathrm{eff}}_{xx}(a,b) = E^{\mathrm{ex1}}E^{\mathrm{ex2}}{}^{*}\omega_{\mathrm{ex}}\,\mathrm{Im}(\chi^{\mathrm{g,ex}})\{10\Delta\chi^{\mathrm{sol}}[\cos(a)\cos(b) + \sin(a)\sin(b)] + \sum_i[\chi^{\mathrm{e}}_{ii}(\omega_{\mathrm{pr}}) - \chi^{\mathrm{g}}_{ii}(\omega_{\mathrm{pr}}) + \chi^{\mathrm{glob}}_{ii}] \times [\cos(a)\cos(b)A^i_x + \sin(a)\sin(b)B^i_x]\} \quad (16)$$

where x stands for the molecular coordinate indices (1, 2, 3): $A^i_1 = B^i_2 = 4 - 2\delta_{i1}$, $A^i_2 = B^i_1 = 3 + \delta_{i1}$, and $A^i_3 = B^i_3 = 4 - \delta_{i1}$. The off-diagonal elements are all zero except for

$$\Delta\chi^{\mathrm{eff}}_{12}(a,b) = \Delta\chi^{\mathrm{eff}}_{21}(a,b) = E^{\mathrm{ex1}}E^{\mathrm{ex2}}{}^{*}\omega_{\mathrm{ex}}\,\mathrm{Im}(\chi^{\mathrm{g,ex}})/2 \times \sum_i[\chi^{\mathrm{e}}_{ii}(\omega_{\mathrm{pr}}) - \chi^{\mathrm{g}}_{ii}(\omega_{\mathrm{pr}}) + \chi^{\mathrm{glob}}_{ii}][\cos(a)\sin(b) + \sin(a)\cos(b)](1 - 3\delta_{i1})\} \quad (17)$$

The observable in the grating experiment is the component of the probe field that is diffracted from the grating described

by $\Delta\chi^{\mathrm{eff}}(a,b)$. This is obtained through the usual constitutive relation for linear polarization:[22]

$$E_i^{\mathrm{sig}}(a,b,c) = i\sum_j \Delta\chi_{ij}^{\mathrm{eff}}(a,b)E_j^{\mathrm{pr}}(c) \tag{18}$$

In the small-crossing-angle approximation the component of the probe field along the optic axis ($\mathbf{u}_3$) is negligible, and the signal field will not exhibit any component along $\mathbf{u}_3$ either. We can then restrict our attention to only fields polarized in the ($\mathbf{u}_1$,$\mathbf{u}_2$) plane.

In the above derivation, the four-wave-mixing process for the transient grating experiment was broken into two distinct steps: a photoselection process by the two excitation fields that creates a spatially varying change in the linear susceptibility of the material, followed by a probe field interaction with this modulated susceptibility that gives rise to a diffracted signal field. This picture provides a useful intuitive basis for assigning the symmetry characteristics of the various physical contributions to the change in susceptibility. However, this formalism does not lead to a natural treatment of phase-matching considerations between the four fields involved. Another disadvantage is that the susceptibility modulation tensor $\Delta\chi_{ij}^{\mathrm{eff}}(a,b)$ is an explicit functional of the two input excitation fields. Since the ultimate goal of this work is to determine the characteristics of the protein only, it is more appropriate to describe the material response in terms of the third-order nonlinear susceptibility tensor elements $\chi_{ijkl}^{(3)}$. The constitutive relation for the field radiated by the third-order polarization is (ignoring constant prefactors):[23]

$$E_l^{\mathrm{sig}}(a,b,c) = i\sum_{ijk}\chi_{ijkl}^{(3)}E_i^{\mathrm{ex1}}(a)E_j^{\mathrm{ex2}}{}^*(b)E_k^{\mathrm{pr}}(c) \tag{19}$$

When eqs 18 and 19 are compared, the relation between the linear and nonlinear susceptibility tensors is

$$\chi_{kl}^{\mathrm{eff}}(a,b) = \sum_{ij}\chi_{ijkl}^{(3)}E_i^{\mathrm{ex1}}(a)E_j^{\mathrm{ex2}}{}^*(b) \tag{20}$$

Since the $\chi_{ijkl}^{(3)}$ must be independent of the polarization angles a and b, the various tensor elements can be identified on the basis of their field-polarization-dependent coefficients. The resulting nonzero elements are

$$\chi_{1111}^{(3)} = \chi_{2222}^{(3)} = \omega_{\mathrm{ex}}\,\mathrm{Im}(\chi^{\mathrm{g,ex}})[10\Delta\chi^{\mathrm{sol}} + \sum_i[\chi_{ii}^{\mathrm{e}}(\omega_{\mathrm{pr}}) - \chi_{ii}^{\mathrm{g}}(\omega_{\mathrm{pr}}) + \chi_{ii}^{\mathrm{glob}}](4 - 2\delta_{i1})] \tag{21}$$

$$\chi_{2211}^{(3)} = \chi_{1122}^{(3)} = \omega_{\mathrm{ex}}\,\mathrm{Im}(\chi^{\mathrm{g,ex}})[10\Delta\chi^{\mathrm{sol}} + \sum_i[\chi_{ii}^{\mathrm{e}}(\omega_{\mathrm{pr}}) - \chi_{ii}^{\mathrm{g}}(\omega_{\mathrm{pr}}) + \chi_{ii}^{\mathrm{glob}}](3 + \delta_{i1})] \tag{22}$$

$$\chi_{1212}^{(3)} = \chi_{2121}^{(3)} = \chi_{1221}^{(3)} = \chi_{2112}^{(3)} = \frac{\omega_{\mathrm{ex}}}{2}\mathrm{Im}(\chi^{\mathrm{g,ex}})\sum_i[\chi_{ii}^{\mathrm{e}}(\omega_{\mathrm{pr}}) - \chi_{ii}^{\mathrm{g}}(\omega_{\mathrm{pr}}) + \chi_{ii}^{\mathrm{glob}}](1 - 3\delta_{i1}) \tag{23}$$

One of the checks on whether the derivation of the nonlinear susceptibilities is correct is to determine whether they satisfy the spatial symmetry relations appropriate for an isotropic medium (i.e., proteins in solution). From Hellwarth, the only nonzero independent elements must satisfy[24]

$$\chi_{1122}^{(3)} = \chi_{2211}^{(3)}$$
$$\chi_{1212}^{(3)} = \chi_{2121}^{(3)}$$
$$\chi_{1221}^{(3)} = \chi_{2112}^{(3)}$$
$$\chi_{1111}^{(3)} = \chi_{2222}^{(3)} = \chi_{1122}^{(3)} + \chi_{1212}^{(3)} + \chi_{1221}^{(3)} \tag{24}$$

Direct substitution of eqs 21−23 into eq 24 verifies that the expressions for $\chi_{ijkl}^{(3)}$ do indeed obey the proper symmetry constraints. Note that of the three unequal and nonzero tensor elements, only two are linearly independent. This means that only two elements need be acquired experimentally to fully characterize the nonlinear susceptibility (at least for the single frequency and time-ordering geometry considered here).[23] It is experimentally simplest to measure $\chi_{1111}^{(3)}$ and $\chi_{1122}^{(3)}$.

Insight into the anisotropic dynamics of the protein can be obtained by grouping the individual microscopic contributions to the grating signals into two categories, "in-plane" and "out-of-plane" relative to the molecular axis:

$$\Delta n_{\mathrm{in}} \equiv \mathrm{Re}[\Delta\chi_{22} + \Delta\chi_{33}]/2$$
$$\Delta n_{\mathrm{out}} \equiv \mathrm{Re}[\Delta\chi_{11}] \tag{25}$$
$$\Delta\alpha_{\mathrm{in}} \equiv \mathrm{Im}[\Delta\chi_{22} + \Delta\chi_{33}]/2$$
$$\Delta\alpha_{\mathrm{out}} \equiv \mathrm{Im}[\Delta\chi_{11}] \tag{26}$$

Here Δn_{in} and $\Delta\alpha_{\mathrm{in}}$ correspond to the (averaged) change in the index and absorption ellipsoids along a direction within the heme plane, while Δn_{out} and $\Delta\alpha_{\mathrm{out}}$ are the components of the change in the index/absorption ellipsoids along the heme normal. There is a proportionality constant implicit in eqs 25 and 26 since the grating signals are in arbitrary units. With these definitions, the third-order susceptibility elements from eqs 21 and 22 can be written (neglecting constant prefactors):

$$\mathrm{Re}[\chi_{1111}^{(3)}] = 8\Delta n_{\mathrm{in}} + 2\Delta n_{\mathrm{out}}$$
$$\mathrm{Re}[\chi_{1122}^{(3)}] = 6\Delta n_{\mathrm{in}} + 4\Delta n_{\mathrm{out}} \tag{27}$$

so the index changes relative to the heme plane are

$$10\Delta n_{\mathrm{in}} = 2\mathrm{Re}[\chi_{1111}^{(3)}] - \mathrm{Re}[\chi_{1122}^{(3)}]$$
$$10\Delta n_{\mathrm{out}} = 4\mathrm{Re}[\chi_{1122}^{(3)}] - 3\mathrm{Re}[\chi_{1111}^{(3)}] \tag{28}$$

with similar relations for the in-plane and out-of-plane changes in absorption. These expressions will be used to relate the grating signals observed in the laboratory to index and absorption changes relative to the heme plane of the protein.

B. Expected Anisotropy from the Change in the Protein Electronic State. The anisotropy $r(t)$ is a normalized measure of how much the transient properties of a material differ between probe fields polarized parallel or perpendicular to the excitation field. The absorption anisotropy is defined as[25,26]

$$r(t) = \frac{\Delta\alpha_{\parallel}(t) - \Delta\alpha_{\perp}(t)}{\Delta\alpha_{\parallel}(t) + 2\Delta\alpha_{\perp}(t)} \tag{29}$$

where the subscripts $\parallel$ and $\perp$ refer to the relative pump/probe polarization. The factor of 2 in the denominator of eq 29 is necessary for proper normalization because there are two directions orthogonal to the excitation polarization and only one parallel. Knowledge of the anisotropy can be used, for example,

to determine quantities such as orientational diffusion times, or for placing constraints on the possible orientations of a given dipole transition. In the case of heme proteins, we are interested in the anisotropy both as a probe of the excited electronic state symmetry in the vicinity of the heme (since this can indirectly be affected by the local protein structure) and as a measure of the dynamics of the asymmetric protein motions.

As determined by Myers and Hochstrasser,[27] the component of the third-order susceptibility that arises from a purely absorptive dipole interaction with anisotropy r_{Im} as defined in eq 29 should obey the following expressions:

$$\mathrm{Im}(\chi^{(3)}_{1111}) = C(1 + 2r_{\mathrm{Im}})/3$$

$$\mathrm{Im}(\chi^{(3)}_{1122}) = C(1 - r_{\mathrm{Im}})/3$$

$$\mathrm{Im}(\chi^{(3)}_{1212}) = Cr_{\mathrm{Im}}/2 \qquad (30)$$

where C is a constant. Inverting this, we can solve for r_{Im} in terms of $\chi^{(3)}_{ijkl}$:

$$r_{\mathrm{Im}} = \frac{\mathrm{Im}(\chi^{(3)}_{1111}) - \mathrm{Im}(\chi^{(3)}_{1122})}{\mathrm{Im}(\chi^{(3)}_{1111}) + 2\mathrm{Im}(\chi^{(3)}_{1122})} \qquad (31)$$

We assume that any absorptive changes arising from structural and thermal effects in the globin or in solution are negligible. Plugging in eqs 21 and 22 for the tensor elements with Im(χ^{glob}) and Im(χ^{sol}) set to 0, eq 31 becomes

$$r_{\mathrm{Im}}(\omega_{\mathrm{pr}}) = \frac{1}{10}\frac{\mathrm{Im}\sum_i[\chi^{e}_{ii}(\omega_{\mathrm{pr}}) - \chi^{\mathrm{g}}_{ii}(\omega_{\mathrm{pr}})](1 - 3\delta_{i1})}{\mathrm{Im}\sum_i[\chi^{\mathrm{e}}_{ii}(\omega_{\mathrm{pr}}) - \chi^{\mathrm{g}}_{ii}(\omega_{\mathrm{pr}})]} \qquad (32)$$

This is a general expression for the absorption anisotropy of a ground-state planar absorber that has arbitrary excited-state absorption symmetry.

To treat the complex grating signals, we need to extend the standard definition of r to include effects that are not simply due to absorptive interactions with the probe field. We define a real counterpart to the absorption anisotropy r_{Im}, which we will refer to as the "phase anisotropy":[9]

$$r_{\mathrm{Re}} \equiv \frac{\mathrm{Re}(\chi^{(3)}_{1111}) - \mathrm{Re}(\chi^{(3)}_{1122})}{\mathrm{Re}(\chi^{(3)}_{1111}) + 2\mathrm{Re}(\chi^{(3)}_{1122})} \qquad (33)$$

Substituting eqs 21 and 22 into eq 33 provides an expression for r_{Re} in terms of individual microscopic susceptibilities:

$$r_{\mathrm{Re}} = \frac{2}{5}\frac{\mathrm{Re}\sum_i[\chi^{\mathrm{e}}_{ii}(\omega_{\mathrm{pr}}) - \chi^{\mathrm{g}}_{ii}(\omega_{\mathrm{pr}}) + \chi^{\mathrm{glob}}_{ii}](1 - 3\delta_{i1})}{4\mathrm{Re}\sum_i[\chi^{\mathrm{e}}_{ii}(\omega_{\mathrm{pr}}) - \chi^{\mathrm{g}}_{ii}(\omega_{\mathrm{pr}}) + \chi^{\mathrm{glob}}_{ii}] + 3\mathrm{Re}\Delta\chi^{\mathrm{sol}}} \qquad (34)$$

This definition allows us to treat changes in the real index of refraction in a manner analogous to that used in the analysis of polarized transient absorption data. Just as the numerical value of the absorption anisotropy is related to the shapes and orientations of the ground- and excited-state absorption ellipsoids, the phase anisotropy contains information about the index ellipsoids. This is of interest primarily because we expect the contribution of protein strain χ^{glob} to the grating signals to be purely real. Protein strain can indirectly contribute to the Im part of the signals through perturbations of the environment in the vicinity of the heme, whose electronic-state contributions to the signals are both anisotropic and complex. The time evolution of the electronic states can also be affected indirectly by conformation changes and thermal relaxation of the protein.[20,21] These effects can contribute to both the Im and Re components of the signal and must be separated through control studies on other systems.

Since the probe experiences a phase shift owing to the different electronic structures of the ligated and deligated states, r_{Re} will in general have a nonzero contribution from the electronic-state population. This can obscure the anisotropy arising from the conformation change. The electronic-state (dipole) contribution to r_{Re} can be isolated by ignoring the structural and thermal contributions, Re(χ^{glob}) and Re(χ^{sol}), to the change in susceptibility at the probe wavelength so that eq 34 has the same form as eq 32, with Im $\rightarrow$ Re. The magnitude of the electronic-state contribution can be estimated by invoking the Kramers−Kronig (KK) relationship between the Re and Im components of the change in the linear susceptibility:[15]

$$\mathrm{Re}[\Delta\chi^{\mathrm{eff}}(\omega)] = -\frac{2}{\pi}P\int_0^{\infty}\frac{\omega'\,\mathrm{Im}[\Delta\chi^{\mathrm{eff}}(\omega')]}{\omega^2 - \omega'^2}\,\mathrm{d}\omega' \qquad (35)$$

where P denotes the Cauchy principal value of the integral. In practice the integration limits in eq 35 are taken to be over the electronic resonances in the near-UV to near-IR wavelength regime to minimize contributions from the bulk protein, which does not absorb strongly in this region. The electronic-state contribution to the phase anisotropy can then be written in terms of the components of the absorption ellipsoid using eqs 2 and 35:

$$r^{\mathrm{elect}}_{\mathrm{Re}}(\omega) = \frac{1}{10}\frac{P\int_0^{\infty}\frac{1}{\omega^2 - \omega'^2}\sum_i[\alpha^{\mathrm{e}}_{ii}(\omega') - \alpha^{\mathrm{g}}_{ii}(\omega')](1 - 3\delta_{i1})\,\mathrm{d}\omega'}{P\int_0^{\infty}\frac{1}{\omega^2 - \omega'^2}\sum_i[\alpha^{\mathrm{e}}_{ii}(\omega') - \alpha^{\mathrm{g}}_{ii}(\omega')]\,\mathrm{d}\omega'} \qquad (36)$$

In general, the excited-state absorption ellipsoid will vary as a function of the time delay t between the excitation and probe pulses. Since the absorption spectrum of photodissociated MbCO nearly converges to that of equilibrium deoxyMb within ~20 ps,[20,28] the polarization characteristics of the electronic state can be assigned on the basis of the known symmetry of the various dipole transitions at equilibrium. This assignment provides constraints on the magnitude of the phase anisotropy r_{Re} that can arise from excited electronic states, valid for time delays 20 ps $< t <$ 10 ns (when rotational diffusion and ligand recombination effects become apparent).[29] At shorter time delays the polarization-resolved transient absorption spectra are not available and no hard limits can be placed on the electronic contribution to r_{Re}.

The equilibrium electronic states of crystalline MbCO and deoxyMb have been investigated thoroughly by others using polarized absorption spectroscopy.[16,30−32] In crystalline form Mb has a well-defined orientation, and measurements can be made along different crystal axes to completely resolve the absorption ellipsoid. The solution spectra are reproducible from the measured crystalline spectra, suggesting that the heme environment is the same in both cases. MbCO's spectrum, in particular,

TABLE 1: Polarizations of the Various Transitions for DeoxyHb and DeoxyMb throughout the near-IR Spectral Range[a]

		α (cm^{-1} M^{-1})		ω_0 (cm^{-1})		$\Delta\omega$ (cm^{-1})	
feature	polarization	Hb	Mb	Hb	Mb	Hb	Mb
band I	*z*	155	112	10900	10620	770	794
band II	*z* (50−75%)	110	109	12250	11760	1200	1738
	x, *y* (25−50%)						
band III	*x*, *y*	150	122	13200	13130	290	306
band IV	*x*, y	90	12	15050	14840	310	407
Q-band	*x*, y	3300	3391	19800	20020	3900	3883

[a] The fit parameters given for deoxyHb are from Eaton et al.[33] The parameters for deoxyMb were determined by fitting the measured isotropic equilibrium spectrum of deoxyMb to the sum of five Gaussian transitions following the approach of ref 33, each of the form $\alpha \exp[-(\omega - \omega_0)^2/\Delta\omega^2]$. The heme electronic transitions are very similar between Hb and Mb, suggesting that the associated polarization assignments between the two species are the same.

is quite simple; all transitions from the N-band (330 nm) through the near-IR (1200 nm) are overwhelmingly polarized in-plane. This is also true for deoxyMb in the range 300−760 nm, but for longer wavelengths the dipole transitions acquire a predominantly out-of-plane component. A summary of the polarizations of the various transitions of deoxyMb and deoxyhemoglobin (deoxyHb) in the visible−near-IR region is shown in Table 1. Detailed information on the transitions underlying the near-IR absorption spectrum of deoxyMb was not readily available from the literature. The spectroscopic assignments for deoxyHb were used instead.[33] It has been shown by others that the electronic configurations of the Fe(II) heme in deoxyHb and deoxyMb are virtually identical.[32]

The measured absorption spectra in solution $\alpha_{iso}(\omega)$ of MbCO and deoxyMb were decomposed into contributions parallel and perpendicular to the heme plane using these literature values of the orientations of the various dipole transitions and the relation[34]

$$\alpha_{iso}(\omega) = \sum_i \alpha_i/3 \tag{37}$$

between the isotropic and polarized absorption coefficients. Here the index *z* refers to the normal to the heme plane and *x* and *y* refer to the in-plane directions (cf., Figure 1).[35] The long-time limiting values of the contributions from electronic transitions to the absorption and phase anisotropies are calculated using eqs 32 and 36, respectively, with $\mathrm{Im}[\chi^{e}_{ii}(\omega_{pr})]$ and $\mathrm{Im}[\chi^{g}_{ii}(\omega_{pr})]$ in eq 32 corresponding to $\omega^{-1}\alpha_i^{deox}(\omega)$ and $\omega^{-1}\alpha_i^{CO}(\omega)$, respectively. Applying these relations to the orientationally decomposed absorption spectra from eq 37 yields the long-time limiting values for the electronic-state contributions to r_{Im} and r_{Re}, shown in Figure 2. There is some uncertainty in the literature values of the relative magnitude of the *z*-polarized component of the band II transition (850 nm), as noted in Table 1, so the extrema of the possible values of the band II absorption ellipsoid are included in the error bars for r_{Re}^{elect} and r_{Im}^{elect} shown in Figure 2. As expected, r_{Im}^{elect} is very close to $^1/_{10}$ throughout the visible spectrum and decreases monotonically to $-^1/_5$ in the near-IR as the absorption acquires more of a *z*-polarized component at these wavelengths. The phase anisotropy r_{Re}^{elect} is also very close to $^1/_{10}$ for most of the visible range where it is dominated by contributions from the strong Soret and Q-band transitions. However, r_{Re}^{elect} deviates significantly from $^1/_{10}$ for $\lambda > 600$ nm, rising to nearly 0.20 at 880 nm before falling to about 0 for $\lambda > 1000$ nm. The rather abrupt "spikes" in r_{Re}^{elect} at several

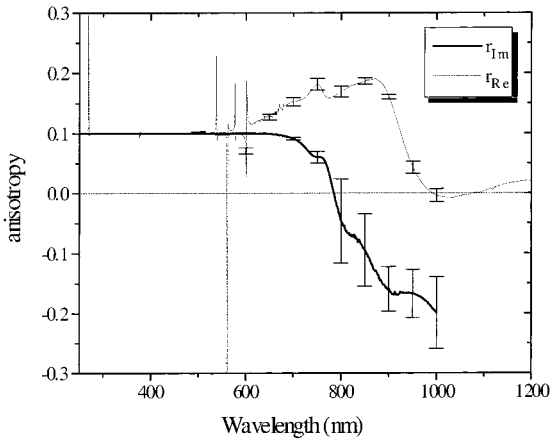

Figure 2. Contribution of the electronic-state change (CO-ligated heme → deoxyheme species) to the absorption and phase anisotropies calculated using the equilibrium absorption data in eqs 32 and 36. Since the change in absorption for $\lambda > 1000$ nm is extremely small, the calculated absorption anisotropy in this range is not shown, as it is dominated by measurement errors. The phase anisotropy in this range, however, is dominated by the contributions from the visible and near-IR transitions and has reasonably low uncertainty. The uncertainties in r_{Im} and r_{Re} arising from the range of likely polarizations of the band II transition (Table 1) are also included in the error bars.

points in the visible range are due to the very small value of the denominator of eq 36 at wavelengths where the in-plane and out-of-plane changes in the index of refraction are of opposite sign. The most likely value for the dipole contribution to the phase anisotropy at our probe wavelength of 800 nm is $r_{Re}^{elect} = 0.17 \pm 0.01$. The absorption anisotropy at 800 nm is changing very rapidly with the relative magnitudes of the *z*- and *x*,*y*-polarized transitions and is expected to be about -0.05 ± 0.10. The large uncertainty in the absorption anisotropy arises mostly from the possible range in the polarization of the band II transition, but experimental error in the spectral measurement contributes somewhat as well, especially for $\lambda > 900$ nm where the change in absorption is extremely small.

The predictions of Figure 2 can be used to identify characteristic features of the electronic-state transition for the reaction MbCO → deoxyMb in different spectral domains. In addition, the magnitudes of the observed anisotropies can be compared with the expected electronic contributions from Figure 2 to determine the presence of nondipole contributions to the phase relaxation.

III. Experimental Section

A. Optical Apparatus. In the transient grating experiment, an ultrafast probe laser pulse is Bragg-diffracted from a photoinduced grating that results from the interference between two excitation pulses crossed within the sample. The diffraction efficiency is monitored as a function of time delay *t* between the probe and excitation pulses. Since both phase gratings as well as amplitude (absorptive) gratings give rise to diffraction, the observed signals will contain more information than a simple pump−probe experiment in which only absorptive changes can be monitored. A phase grating results if the microscopic contributions ($\Delta\chi^{sol}$, $\Delta\chi^{glob}$, $\Delta\chi^{elect}$) to the third-order susceptibility are purely real, and an amplitude grating results if they are purely imaginary. In general, of course, they are complex and the grating signals have contributions from both absorptive and index changes.

These contributions cannot be distinguished by direct detection but can be easily separated using optical heterodyne

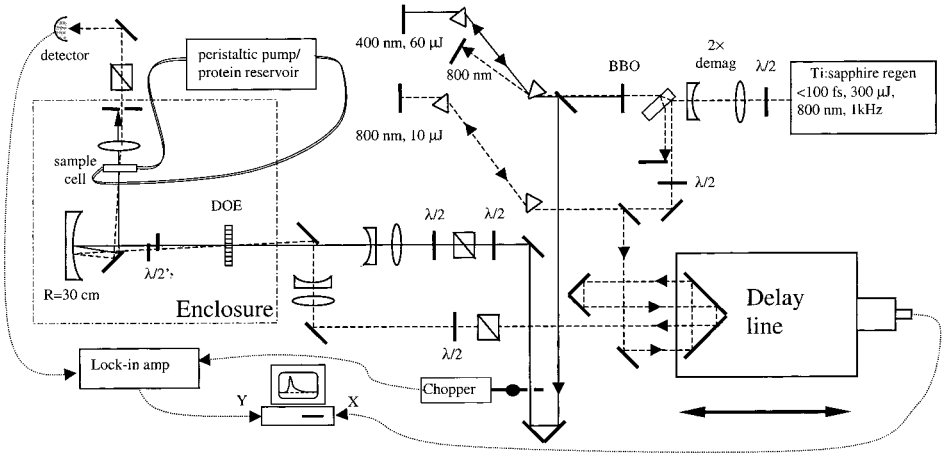

Figure 3. Apparatus for the OHD transient grating experiments: (dashed lines) 800 nm beams; (solid lines) 400 nm beams; $\lambda/2$, half-wave plate; DOE, diffractive optical element; BBO, 300 μm thick β-barium borate crystal for second harmonic generation. The 400 and 800 nm beams are brought to loose foci on the surface of the DOE with individual telescopes in each arm.

detection (OHD). OHD involves spatially and temporally overlapping a coherent reference field with the signal field of interest on a detector.[36] The OHD signal is the interference term between the two fields, which can be isolated by making the reference amplitude much larger than the signal field, modulating the excitation beams, and using lock-in detection to eliminate the static contribution from the reference. For time delays much greater than the pulse widths the OHD signal can be written approximately as[37−39]

$$V_{\mathrm{OHD}}(t) \approx 2A_{\mathrm{ref}}I_{\mathrm{ex}}I_{\mathrm{pr}}|\chi^{(3)}_{ijkl}(t)|\cos[\phi_{\mathrm{ref}} - \phi_{\mathrm{sig}}(t)] \quad (38)$$

where V_{OHD} is the detector output with the reference present and it is assumed that the reference field is a replica of the probe field except for its relative amplitude $A_{\mathrm{ref}} = |E_{\mathrm{ref}}/E_{\mathrm{pr}}|$. I_{ex} and I_{pr} are the intensities of the excitation and probe fields, and the phase difference between the reference and signal fields is

$$\phi_{\mathrm{ref}} - \phi_{\mathrm{sig}}(t) = \phi_{\mathrm{ref}} - \pi/2 - \phi_{\chi}(t) - \phi_{\mathrm{pr}} - \phi_{\mathrm{ex1}} + \phi_{\mathrm{ex2}} = \Delta\phi - \phi_{\chi}(t) \quad (39)$$

Here $\phi_{\chi}(t)$ is the delay-dependent phase of the effective third-order nonlinear response function $\chi^{(3)}_{ijkl}(t)$ (related to the Fourier transform of the third-order nonlinear susceptibility),[23] and $\Delta\phi$ is the phase difference between the input fields. The benefits of OHD are amplification of the signal field, which can lead to a dramatic improvement in the signal-to-noise (S/N);[36] linear dependence of the observable on the signal field amplitude, eliminating cross-terms between different physical contributions, and most importantly, phase-sensitive detection, enabling measurement of the full amplitude and phase of the complex signal field rather than simply its magnitude.

The primary difficulty in implementing OHD experimentally is controlling the relative phase between the reference and signal, $\phi_{\mathrm{ref}} - \phi_{\mathrm{sig}}(t)$. If this phase is allowed to vary randomly over the time scale of data collection, the experimental signal will be distorted. A conventional approach to this problem is to actively lock the phase using the output of an interferometer as the error signal for a feedback loop that controls the position of one of the optics in the input beam paths.[22,40,41] Results published to date using this approach in grating experiments have demonstrated only very limited capabilities for quadrature detection.[42,43] Some of the limitations in these earlier studies arose from the large amount of phase noise (20°), which is more apparent for in-quadrature detection than for in-phase detection.[42] But, more fundamentally, this earlier work is hampered by the requirement for a large signal field to generate easily observable interference patterns to provide an error signal for the feedback loop. Heterodyne detection of weak, in-quadrature signal fields via this approach is nontrivial.

As discussed above, a new method has been developed recently for passive phase stabilization of OHD transient grating signals using a diffractive optical element (DOE) to generate the appropriate input beam patterns.[9,11,12,44−46] Compared with active-feedback methods, this approach is easier to implement and yields improved signal-to-noise, enabling full quadrature detection capability. A schematic of our experimental apparatus is shown in Figure 3. The laser source for this work was a 1-kHz repetition rate, regeneratively amplified Ti:sapphire laser that emitted <100 fs, 300 μJ pulses centered at 800 nm. The 800 nm pulses were frequency-doubled with ∼40% conversion efficiency in a 300 μm thick BBO crystal to generate 400 nm excitation pulses. About 10% of the incident fundamental beam was split off before the doubling crystal to serve as the probe and reference pulse by reflection from the front surface of an uncoated window. The time delay between the 800 nm and the 400 nm pulses was set using a hollow retroreflector mounted on a computer-controlled translation stage driven by a stepper motor (Daedal, Inc.). The delay line was double-passed to increase the maximum delay range from 2.5 to 5 ns. Both the 400 nm and the 800 nm pulses were passed through separate dispersive delay lines consisting of a double-passed prism pair.[47] This imposed a negative frequency chirp on the pulses to precompensate for dispersion in the optics downstream, so that they were near-transform-limited at the sample position. The polarizations of both pulses were set to about one part in 10^2-10^3 at the sample position using Glan−Taylor calcite polarizers placed before the DOE. The relatively low contrast ratio arose from depolarization in the waveplates and mirrors between the polarizers and the sample. The resulting error in the measured anisotropy due to this depolarization is on the order of 1%.

The diffractive optic was a square-modulated, surface-relief element optimized for >30% diffraction efficiency into each of the ±1 diffractive orders at 527 nm (National Optics Institute). The efficiency into each of the ±1 orders was >15% throughout the 400−1000 nm range, so the same element could be used for experiments with tunable probe and excitation wavelengths.

An expanded view of the optical setup using the DOE is shown in Figure 4. Two separate telescopes brought the two

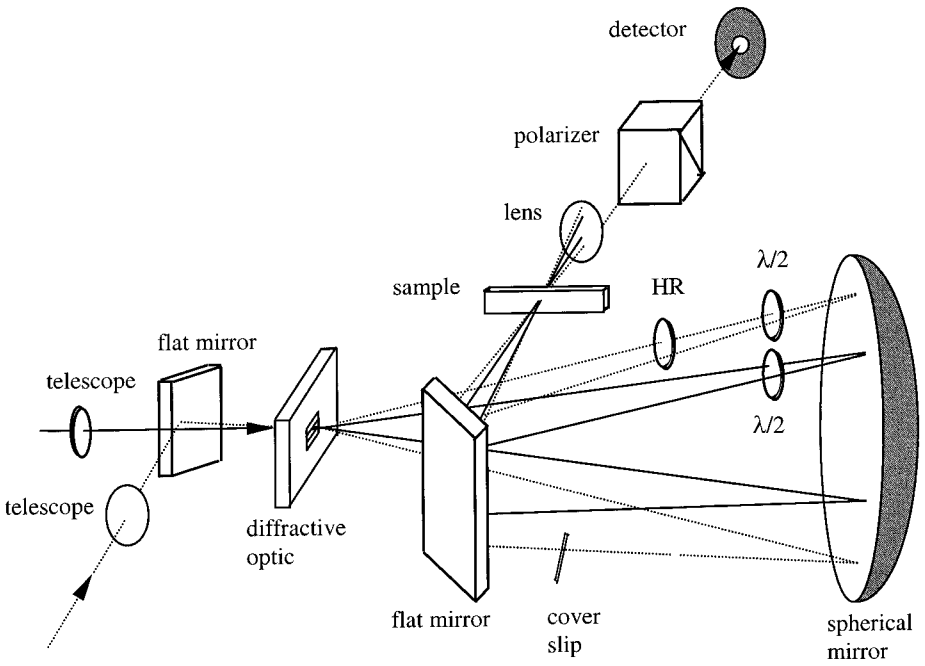

Figure 4. Perspective view of the optical apparatus within the enclosure for the polarization-resolved heterodyne-detected transient grating experiments: (dashed lines) 800 nm beams; (solid lines) 400 nm beams; HR, high-reflector (99.9%) broad band mirror. There is also additional glass in the beam lines (not shown in this figure) to match the group delays within each pulse pair.

different wavelength beams to loose foci onto the same point at the surface of the DOE (200 μm diameter spot for the blue, 100 μm diameter for the IR). The crossing angle between the two beams was small ($\sim$2°) but finite to minimize nonlinear coupling between the two pulses in the DOE substrate. The input pulse energies were kept below 10 μJ/beam at the DOE to avoid continuum generation in the 3/16 in. thick DOE substrate. The DOE split both the 400 and 800 nm pulses into two ($\pm$1 orders), and all other orders were spatially filtered before the sample. The diffraction plane was perpendicular to the crossing plane of the two input beams, as shown in Figure 4. The resulting four pulses were achromatically imaged onto the sample using a 30 cm radius, Al-coated spherical mirror at a 1:1 conjugate ratio, where there are no geometric aberrations from the large angular spread between beams. The spherical mirror was tilted slightly off-axis to separate the incoming from the outgoing beams. A flat mirror was used to pick off the reflected beams and send them toward the sample.

The two replicas of the 400 nm excitation pulse overlapped at a 5.7° angle within the sample to create a holographic interference pattern with a fringe spacing of 4.0 μm. The protein was photodissociated in the illuminated fringes and unchanged in the dark fringes, so that the complex index of refraction varied between them. One of the replicas of the 800 nm pulse (the probe pulse) was Bragg-diffracted from this photoinduced grating through an analyzer polarizer and into the detector (a silicon photodiode). The other 800 nm pulse replica passed through the sample and overlapped with the diffracted signal field on the detector to provide a reference field for OHD.[11,46] The phase-matching condition for Bragg diffraction of the probe pulse from the grating formed by the excitation pulses is automatically satisfied in this geometry.[13,48]

A 200 μm thick coverslip in the probe beam path could be tilted slightly to provide fine control over the path length difference and thus the relative phase between the probe and reference pulses, so that both the real and imaginary components of $\chi^{(3)}$ could be measured. The reference intensity was attenuated by a factor of $\sim 10^3$ by a broad-band 0° dielectric mirror to optimize the signal-to-noise ratio[36] and avoid saturating the detector. Zero-order achromatic half-waveplates in each of the beam paths allowed independent adjustment of all four field polarizations. Additional glass (not shown in Figure 4) was placed in the beam paths as necessary to overlap the time delays between the two excitation pulses and between the probe and reference pulses.

The phase noise has been measured to be about 2.5° rms using excitation and probe beams of the same wavelength.[11] For this case, beams of the same diffractive order (+1 or −1) were diffracted by the DOE into the same direction, and thus were separated by only a few millimeters at any point. Fluctuations in the phase difference $\Delta\phi$ arising from air currents in this case were very small since adjacent beams experienced roughly the same turbulence, giving rise to nearly equal phase distortions that canceled one another in eq 39. In the setup used to measure the protein dynamics, the probe and excitation were of different wavelengths and thus all four of the beams diffracted from the DOE were separated by several centimeters at the spherical mirror. This resulted in increased sensitivity of $\Delta\phi$ to air currents, requiring that an enclosure be placed around the apparatus to reduce the phase noise to $\sim$5° rms. These phase fluctuations were responsible for the bulk of the experimental noise in the protein studies. The phase stability attained here using the DOE is an order of magnitude better than that reported recently by a group using an active feedback scheme.[42]

The measured voltage signals from the lock-in amplifier are not rigorously proportional to the TG signal field as is implied by eq 38. There will always be a contribution from the modulus square of the signal field in addition to the heterodyne term. This contribution can be eliminated by subtracting two sets of data acquired with a π-phase shift between them, so that the sign of the OHD term (eq 38) changes while the sign of the term quadratic in the signal field does not.[49] This procedure also eliminates a pump−probe artifact that arises from passage of the reference beam through the photoexcited sample volume. However, the amplitude and phase modulations imposed on the reference field upon passage through the excited volume will

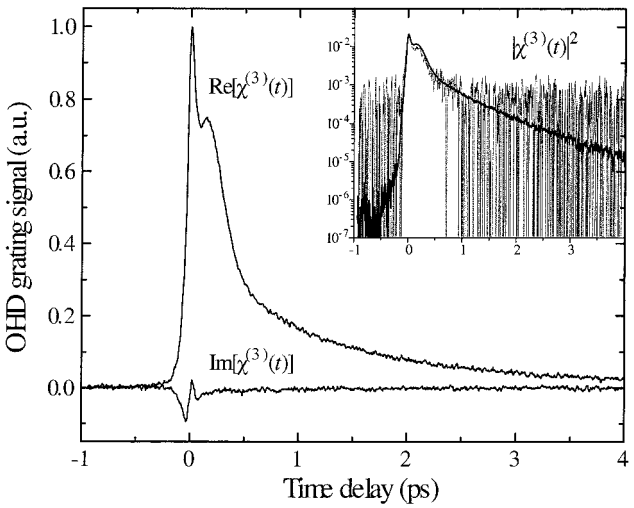

Figure 5. OHD grating signals from liquid CS_2. The inset shows the corresponding direct-detected signal measured under the identical experimental conditions with the reference beam blocked (dotted curve) and normalized to the same scale as the OHD signals. The solid curve in the inset is the modulus-square of the OHD data constructed from $\mathrm{Re}[\chi^3(t)]^2 + \mathrm{Im}[\chi^3(t)]^2$. This comparison illustrates the improvements in S/N with heterodyne detection over direct detection.

still affect the OHD term. By examining the magnitude of the pump−probe modulation of the reference intensity, the amplitude modulation of the OHD signal was found to be <1%. The phase modulation was estimated to be <1° from a measurement of the absolute diffraction efficiency of the reference from the photoinduced grating.[50] Both amplitude and phase modulations are lower than the random experimental noise and can be safely ignored in our experiments. However, this is not universally the case and should be checked for different samples and excitation conditions.

B. Setting the Field Phases. To measure unambiguously the real and imaginary components of the nonlinear susceptibility, the phase difference $\Delta\phi$ between the input fields must be set independently. Since the only experimental observable is $[\phi_\chi(t) - \Delta\phi]$, which includes the phase shift from the nonlinear susceptibility, it is a nontrivial problem to unambiguously set the field phases at the sample position. This is an issue for any OHD experiment—whether actively or passively phase-stabilized—in which none of the input pulses are copropagating, so that their path lengths to the sample and thus their relative phases are not precisely known. However, if at some delay the phase of $\chi^{(3)}_{ijkl}(t)$ can be inferred on the basis of previous knowledge of the material, this can be used to set the field phase difference $\Delta\phi$ and thus enable measurement of $\chi^{(3)}_{ijkl}(t)$ at all delays.

For example, a particularly simple case is impulsive stimulated Raman scattering[51] of 800 nm pulses from liquid carbon disulfide (CS_2). Since CS_2 is almost completely transparent to 800 nm light, the photoinduced change in absorption arising from nonresonant excitation of low-frequency (<500 cm^{-1}) Raman-active modes can be assumed to be negligible for time delays much greater than the laser pulse width. The imaginary component is orders of magnitude smaller than the real component at these time delays and is outside our detection limit, i.e., to an excellent approximation $\phi_\chi(t \gg 0) = 0$. Adjusting the coverslip in the probe beam so that $V_{\mathrm{OHD}}(t \gg 0) = 0$ then results in the phase observable $[\phi_\chi(t \gg 0) - \Delta\phi] = \pi/2$, so that $V_{\mathrm{OHD}}(t) \propto \mathrm{Im}[\chi^{(3)}_{ijkl}(t)]$ at all delays. Thus, the two OHD signals shown in Figure 5 correspond to the Re and Im parts of $\chi^{(3)}_{1111}(t)$. In the inset of Figure 5, these signals are squared and added together for comparison with the direct-detected signal under the same conditions to demonstrate the improvement in S/N under OHD.

For the protein studies, the response was complex and there was no clear delay at which either the Re or Im part of $\chi^{(3)}_{ijkl}(t)$ could be assumed to be nonzero. Instead, the Re and Im signal components were identified on the basis of the presence or absence, respectively, of photoacoustic oscillations on nanosecond time scales.[9] These sinusoidal oscillations in the signal arise from a standing acoustic wave that is driven generally by thermal expansion of the solvent,[52] although global structure changes in the protein may contribute as well.[53] Since these waves are simply density fluctuations, to a good approximation they change only the real part of the refractive index.[54,55] With this in mind, $\Delta\phi$ was set to $\pm\pi/2$ by tilting the coverslip in the probe beam to eliminate the acoustics, so that the observed signals were proportional to the Im component of the protein response. The Re component was then measured separately by imposing a $\pi/2$-phase shift on the probe so that $\Delta\phi$ was either 0 or π.

This $\pi/2$-phase shift was set using a coverslip mounted on a rotation stage at a ~5° angle with respect to the axis of rotation. The axis of rotation was at an angle of a few degrees to the incident beam, so that very small changes in the angle of incidence could be dialled in by rotating the stage a set amount. The phase shifts arising from precession of the surface normal upon rotation about a given angle were calibrated on the basis of the OHD TG signals from a solution of Malachite Green dye, whose response after ~10 ps is almost entirely thermal and thus real.[52] This procedure provides about 5° accuracy in setting the phase. This was further improved in the protein experiments by averaging the results of four data sets acquired with fresh alignments. As a consistency check, the Re and Im components of the MbCO response were squared and added together for comparison with the direct-detected signals measured with the reference beam blocked. The overlap of the two responses showed the OHD signals were linear in the signal field amplitude and in-quadrature with one another as expected.[9] The disagreement between the two traces in the inset of Figure 5 at early time delays arises from the different functional forms for the convolution with the driving field envelopes for the two cases (which was neglected in eq 39).[37−39]

The greatest utility of the OHD technique is on time scales both much longer and much shorter than those over which photoacoustics can be observed. On these time scales there is no clear indication of the phase of the signal field, and absorptive changes cannot be clearly distinguished from index changes. Use of the photoacoustics to provide a marker for setting the reference phase enables separation of the Re and Im components over all time scales, where new details of the protein response can be observed [e.g., from inertial motions to ligand diffusion out of the protein and bimolecular recombination (10^{-13}−10^{-2} s)].[12]

IV. Conclusion

The analysis and description of the experimental techniques presented here provide the groundwork for discussion and interpretation of heterodyne-detected grating signals from heme proteins. The analysis of the information contained within the experimental signals closely relates the linear and nonlinear optical properties of the material. In particular, the phase anisotropy has been introduced as a quantitative metric for the presence of non-electronic-state contributions to the grating signals.

In the second paper of this series,[14] the complex four-wave-mixing response of carboxymyoglobin will be presented and analyzed in detail. Photoinduced strain in the globin can be isolated from other signal contributions by using the analytic and experimental techniques described here. In particular, decomposition of the grating signals along different molecular coordinates indicates the development of anisotropic protein strain on subpicosecond time scales. This illustrates the fundamental role of collective protein motions in transducing the energy liberated by the heme−CO bond break into protein structure changes.

These observations are made possible through the introduction of diffractive optics as a simple means to execute heterodyne detection for the separation of the real and imaginary components to four-wave-mixing experiments. The experimental heterodyne technique using a diffractive element to generate the appropriate beam pattern is simpler and more robust than alternative methods employing active phase-locking. The high sensitivity achieved through the interferometric nature of this experiment may provide a general procedure using off-resonance probes for following the bath dynamics that are essential to a detailed understanding of reactions in the condensed phase.

Acknowledgment. This work was supported by the Natural Sciences and Engineering Research Council of Canada and Photonics Research Ontario. We would like to dedicate this paper and the companion paper (part 2) to Kent Wilson in tribute to his many contributions to femtosecond spectroscopy and to his zest for science that has been an inspiration to us all.

References and Notes

(1) Frauenfelder, H.; Sligar, S. G.; Wolynes, P. G. *Science* **1991**, *254*, 1598.

(2) This problem is very similar to the protein folding problem. See overview on Leventhal's paradox in: Dill, K. A. *Curr. Opin. Struct. Biol.* **1993**, *3*, 99.

(3) Miller, R. J. D. *Acc. Chem. Res.* **1994**, *27*, 145.

(4) Antonini, E.; Brunori, M. *Hemoglobin and Myoglobin in their Reactions with Ligands;* North-Holland Publishing: Amsterdam, Netherlands, 1971. Dickerson, R. E.; Geis, I. *HemoglobIn Structure, Function, Evolution, and Pathology*; Benjamin Cummings Publishing: Menlo Park, CA, 1983.

(5) Monod, J.; Wyman, J.; Changeux, J. P. *J. Mol. Biol.* **1965**, *12*, 88.

(6) Perutz, M. F. *Nature* **1970**, *228*, 726.

(7) Gelin, B. R.; Karplus, M. *Proc. Natl. Acad. Sci. U.S.A.* **1977**, *74*, 801.

(8) Srajer, V.; Teng, T.; Ursby, T.; Pradervand, C.; Ren, Z.; Adachi, S.; Schildkamp, W.; Bourgeois, D.; Moffat, K. *Science* **1996**, *274*, 1726.

(9) Goodno, G. D.; Astinov, V.; Miller, R. J. D. *J. Phys. Chem. B* **1999**, *103*, 603.

(10) Seno, Y.; Go, *N. J. Mol. Biol.* **1990**, *216*, 111.

(11) Goodno, G. D.; Dadusc, G.; Miller, R. J. D. *J. Opt. Soc. Am. B* **1998**, *15*, 1791.

(12) Dadusc, G.; Goodno, G. D.; Chiu, H. L.; Ogilvie, J.; Miller, R. J. D. *Isr. J. Chem.* **1998**, *38*, 191.

(13) Rogers, J. A.; Nelson, K. A. *Physica B* **1996**, *219&220*, 562.

(14) Goodno, G. D.; Astinov, V.; Miller, R. J. D. *J. Phys. Chem. A* **1999,** *103*, 10630.

(15) Saleh, B. E. A.; Teich, M. C. *Fundamentals of Photonics;* John Wiley & Sons: New York, 1991; pp 176−179.

(16) Eaton, W. A.; Hofrichter, J. *Methods Enzymol.* **1981**, *76*, 175.

(17) Marion, J. B.; Thornton, S. T. *Classical Dynamics of Particles and Systems*, 3rd ed.; Harcourt Brace Jovanovich: San Diego, 1988; p 384.

(18) Yariv, A. *Optical Electronics*, 4th ed.; Saunders College Publishing: Philadelphia, 1991; p 5.

(19) Deeg, F. W.; Fayer, M. D. *J. Chem. Phys.* **1989**, *91*, 2269.

(20) Lim, M.; Jackson, T. A.; Anfinrud, P. A. In *Ultrafast Phenomena VIII*; Martin, J.-L., Migus, A., Mourou, G. A., Zewail, A. H., Eds.; Springer-Verlag: Berlin, 1993; p 522.

(21) Lim, M.; Jackson, T. A.; Anfinrud, P. A. *J. Phys. Chem.* **1996**, *100*, 12043.

(22) Eichler, H. J.; Gunter, P.; Pohl, D. W. *Laser-Induced Dynamic Gratings*; Springer-Verlag: Berlin, 1986.

(23) Butcher, P. N.; Cotter, D. *The Elements of Nonlinear Optics*; Cambridge University Press: Cambridge, 1991.

(24) Hellwarth, R. W. *Prog. Quantum Electr.* **1977**, *5*, 1.

(25) Magde, D. *J. Chem. Phys.* **1978**, *68*, 3717.

(26) Kliger, D. S.; Lewis, J. W.; Randall, C. E. *Polarized Light in Optics and Spectroscopy*; Academic Press: Boston, MA, 1990.

(27) Myers, A. B.; Hochstrasser, R. M. *IEEE J. Quantum. Electron.* **1986**, *22*, 1482.

(28) Petrich, W. J.; Poyart, C.; Martin, J. L. *Biochemistry* **1988**, *27*, 4049.

(29) Albani, J.; Alpert, B. *Chem. Phys. Lett.* **1986**, *131*, 147.

(30) Eaton, W. A.; Hochstrasser, R. M. *J. Chem. Phys.* **1968**, *49*, 985.

(31) Churg, A. K.; Makinen, M. W. *J. Chem. Phys.* **1978**, *68*, 1913.

(32) Makinen, M. W.; Churg, A. K. In *Iron Porphyrins, Part I*; Lever, A. B. P., Gray, H. B., Eds.; Addison-Wesley: Reading, MA, 1983; p 141.

(33) Eaton, W. A.; Hanson, L. K.; Stephens, P. J.; Sutherland, J. C.; Dunn, J. B. R. *J. Am. Chem. Soc.* **1978**, *100*, 4991.

(34) Berne, B. J.; Pecora, R. *Dynamic Light Scattering*; John Wiley & Sons: New York, 1976; p 152.

(35) The molecular coordinates (x, y, z) are referred to within equations by the numerical indices (2, 3, 1), respectively. For example, δ_{i1} in eq 33 is nonzero only for the z-polarized transition.

(36) Levenson, M. D.; Eesley, G. L. *Appl. Phys.* **1979**, *19*, 1.

(37) McMorrow, D.; Lotshaw, W. T.; Kenney-Wallace, G. A. *IEEE J. Quantum Electron* **1988**, *24*, 443.

(38) Dickson, T. R. In Ph.D. Dissertation, Physics Department, University of Toronto, Toronto, Ont., 1991; p 151.

(39) Vohringer, P.; Scherer, N. F. *J. Phys. Chem.* **1995**, *99*, 2684.

(40) Scherer, N. F.; Carlson, R. J.; Matro, A.; Du, M.; Ruggiero, A. J.; Romero-Rochin, V.; Cina, J. A.; Fleming, G. R.; Rice, S. A. *J. Chem. Phys.* **1991**, *95*, 1487.

(41) de Boeij, W. P.; Pshenichnikov, M. S.; Wiersma, D. A. *Chem. Phys. Lett.* **1995**, *247*, 264.

(42) Matsuo, S.; Tahara, T. *Chem. Phys. Lett.* **1997**, *264*, 636.

(43) Chang, Y. J.; Cong, P.; Simon, J. D. *J. Phys. Chem.* **1995**, *99*, 7857.

(44) Goodno, G. D.; Miller, R. J. D. In *International Quantum Electronics Conference*; Vol. 7, OSA Technical Digest Series; Optical Society of America: Washington, DC, 1998; p 101.

(45) Goodno, G. D.; Astinov, V.; Miller, R. J. D. In *Ultrafast Phenomena XI*; Elsaesser, T., Fujimoto, J. G. Wiersma, D. A., Zinth, W., Eds.; Springer Series in Chemical Physics; Springer: Berlin, 1998; No. 63, p 130.

(46) Maznev, A. A.; Nelson, K. A.; Rogers, J. A. *Opt. Lett.* **1998**, *23*, 1319. Koehl, R. M.; Adachi, S.; Nelson, K. A. In *Ultrafast Phenomena XI*; Springer Series in Chemical Physics; Elsaesser, T., Fujimoto, J. G. Wiersma, D. A., Zinth, W., Eds.; Springer Series in Chemical Physics; Springer: Berlin, 1998; No. 63, p 136.

(47) Fork, R. L.; Martinez, O. E.; Gordon, J. P. *Opt. Lett.* **1984**, *9*, 150.

(48) Maznev, A. A.; Crimmins, T. F.; Nelson, K. A. *Opt. Lett.* **1998**, *23*, 1378.

(49) Palese, S.; Schilling, L.; Miller, R. J. D.; Staver, P. R.; Lotshaw, W. T. *J. Phys. Chem.* **1994**, *98*, 6308.

(50) Kogelnik, H. *Bell Syst. Technol. J.* **1969**, *48*, 2909.

(51) Ruhman, S.; Kohler, B.; Joly, A. G.; Nelson, K. A. *IEEE J. Quantum Electron.* **1988**, *24*, 470.

(52) Nelson, K. A.; Miller, R. J. D.; Lutz, D. R.; Fayer, M. D. *J. Appl. Phys.* **1982**, *53*, 1144.

(53) Genberg, L.; Richard, L.; McLendon, G.; Miller, R. J. D. *Science* **1991**, *251*, 1051. Genberg, L.; Heisel, F.; McLendon, G.; Miller, R. J. D. *J. Phys. Chem.* **1987**, *91*, 5521.

(54) Miller, R. J. D. In *Time-Resolved Spectroscopy*: Clark, R. J. H., Hester, R. E., Eds.; Advances in Spectroscopy Vol. 18; John Wiley and Sons: New York, 1989; p 1.

(55) Nelson, K. A.; Casalegno, R.; Miller, R. J. D.; Fayer, M. D. *J. Chem. Phys.* **1982**, *77*, 114.